Click to see slides of oral presentation

An Efficient Workflow for Geological Characterization in Unconventional Reservoirs from a New Through-the-Bit Logging Electrical Micro-Imaging Tool*

Shiduo Yang[1], Patrick McBride[2], Josselin Kherroubi[1], Alexis He[1], Isabelle Le Nir[1], Daniel Quesada[1], Redha Hasan AI Lawatia[1], and Andy Wray[1]

Search and Discovery Article #42334 (2018)**
Posted December 31, 2018

*Adapted from extended abstract based on oral presentation given at 2018 International Conference and Exhibition, Cape Town, South Africa, November 4-7, 2018
Please see closely related article, "An Improved Approach for Structural Delineation with Multiple Reverse Faults from Borehole Image Dips in Compressional Stress Regime", Search and Discovery article #42335.
 DOI:10.1306/42334Yang2018

[1]Schlumberger, Clamart, Ile-de-France, France (syang4@slb.com)
[2]Tapstone Energy, Oklahoma City, United States

Abstract

It has been proved that the well production in unconventional reservoirs is controlled by reservoir quality and completion quality. The lateral heterogeneity is influenced by the structural complexity, fracture distribution, and facies variation. The fracture evaluation is one of the key elements for optimizing completion design and multiple stage hydraulic fracturing operations. High-resolution borehole images are the established and efficient tools for fracture evaluation. The major challenges are the associated risk of wireline logging in horizontal wells and the relatively lower rate of drilling penetration required in logging while drilling borehole imaging. We propose a solution for accurate fracture evaluation with structural delineation in unconventional reservoirs using a novel borehole resistivity image.

In horizontal wellbores, bedding boundaries are usually parallel to well trajectory, making bed boundary identification difficult due to the lack of clear sinusoidal signatures in the log view. A true-dip plane-based dip picking algorithm has been developed and applied on a new through-the-bit borehole resistivity image (TBEI) for bed boundary picking of different shapes, such as bull's eye, reverse bull's eye and wellbore parallel bedding features. Lithology-bound fractures can also be picked and classified in conjunction with this new method, enabling more accurate fracture characterization within the modeled structure. In our case study, fracture aperture computation from the TBEI is verified by the resistivity image from the FMI™ full-bore formation micro-imager run in the same well.

Although the structures in many unconventional reservoirs are relatively flat, there are still many small-scale, sub-seismic structures and faults controlling the fracture distribution. The near-well structure can be reconstructed from the bed boundaries and faults with an improved structural modeling method. The relationship between fractures and geological structures and faults is then analyzed for optimization of completion design. Breakout and drilling induced fractures can also be confidently identified from the TBEI image and used to determine the stress regime for consideration in hydraulic stimulation.

A case study has been used to demonstrate the benefits of this innovative, new borehole image-based workflow to an unconventional reservoir in the STACK Play of the Anadarko Basin, Oklahoma, USA. The enhanced understanding of natural fracture distribution along the horizontal wellbore, through more accurate structural delineation, to ultimately optimize completion performance and well productivity.

The new TBEI imager consists of three sondes containing 12 pads with 12 buttons per pad, one power supply cartridge and three acquisition cartridges with an inclinometer module from accelerometers (Bammi at al., 2016). The tool mechanics are significantly improved in terms of tolerance of conveyance with only 2.125-in. outer diameter.

The measurement principle used by this new tool is similar to that of the FMI microimager. The alternating electric field current generated from upper insulated section with low frequency travels symmetrically from pads, conductive mud and formation back to upper/lower return electrodes (Figure 1). The passive focusing technology is used to resolve high-resolution features of formation resistivity by maintaining the same EMEX (*émetteur d'excitation*, excitation transmitter*)* potential on all pad surfaces including buttons and metallic surfaces. The tool response consists of two components: a low frequency component modulated by the conductivity of the formation at the depth of investigation (Doll, 1951) and a high-resolution component modulated by the formation micro-conductivity in the very shallow near-wellbore region directly in front of each button.

Speed Correction for Long-Spaced Multiple Sondes

Speed correction is very challenging for the image measurement from this tool because of the six different pad levels and more than 66-inch distance between the closed two sondes. The speed correction designed for continuous wireline logging with a Kalman-filter and is not suitable for through-the-bit logging with pipe changes. A new speed correction has been developed to incorporate the pipe changes and is based on time domain data directly (Figure 2). The pipe changing interval is calculated from measured acceleration, and sticking zones are identified accurately in each of logging intervals.

True Dip-Based Dip Picking in a Horizontal Well

In a horizontal well the shape of most bed boundary dips is not sinusoidal, but appears as a bull’s eye, reverse bull’s eye, or wellbore parallel bedding features. The conventional dip-picking method cannot handle these shapes properly. A new dip picking based on true dip matches the intersection of a plane with the borehole, considering the variations of the borehole deviation and azimuth. Three points are manually picked on the borehole image to define a true plane dip. Each point is translated into spatial coordinates (in true dip space), and the triplet defines a spatial plane (Figure 3a).

The continuous points can be picked by following the image features and a potential trend is also displayed as reference (Figure 3b). The true dip is calculated automatically by following the continuous picked points.

Formation Correlation Analysis with True Stratigraphic Thickness Index

The drilling polarity is easily computed based on the angle between the well trajectory and the pole of formation dip (Figure 4a). When this angle is more than 90°, it indicates drilling down; an angle less than 90° indicates drilling up. Then the true stratigraphic thickness (TST) is computed from apparent formation dip and drilling polarity accordingly with following equation:

$$TST[i] = \begin{cases} TST[i-1] + (MD[i] - MD[i-1]) \times cos(\alpha[i-1]), (DrillingDown) \\ TST[i-1] - (MD[i] - MD[i-1]) \times cos(\alpha[i]), (DrillingUp) \end{cases}$$

where i is each position of picked dip,
MD is measurement depth and,
α is the angle between well trajectory and the pole of formation dip in Figure 4-b.

After the TST computation, the gamma ray (GR) or other logs can be displayed in TST reference. The log response can be varied for the same layer along a long horizontal section but usually the relatively high clay content layers are stable, and the lithology overlaying pattern is comparable (Figure 6). We assume that the thickness of the same layer bedded by a high clay content layer is relatively stable in the near wellbore region. Any thickness change is likely caused by the fault or uncorrected dips. A fault can be easily identified from the borehole image and the dip should be adjusted accordingly. The formation correlation can be achieved by adjusting the two sides of the fault by following the above rules, and then the fault throw can be estimated from TST change as well as the fault type identification (Figure 6).

Quick Structural Delineation with Picked Dips and Faults

To achieve a more realistic geological cross section with continuous formation layering, a novel solution is applied with following steps (Ma et al., 2018):

1) Dips are picked automatically from images in horizontal wells using the true dip-based method. Structure analysis is employed using the automatic structure zonation based on the great circle-fitting criteria.

2) The fault throw is estimated based on correlation analysis of changing TST, and the fault type can be identified by combining the fault dip picked from the image. The fault ordering is done based on the estimated fault throw after one of the major faults is selected as the major projection plane.

3) All dips are projected along the major fault plane vertically by following the similar or parallel fold principle (Etchecopar and Bonnetain, 1992; Yamada et al., 2016); then the projected dips are projected into the plane perpendicular to structural axis or a user-defined cross section. If the cross section is not perpendicular to the structural axis, the projected dips are projected again along with structural axis.

4) After the display layer is defined, the fault throw is applied for the layers and truncated by the extended fault plane. For each truncated area, a B-spline method is applied ensure smoothed layers.

Fracture Evaluation from Borehole Images

Including aperture estimation in fracture evaluation is critical for unconventional reservoir characterization. Because the TBEI imager is based on the same measurement principle as the FMI imager, the fracture aperture computation parameters were kept the same with reverse forwarding modeling in one well logged with the FMI imager and the new TBEI (Figure 5). The fracture aperture difference is less than 10% statistically for the same fractures in the same interval based on mean values.

In Figure 5, we can see that there is little difference for each of fracture segment's aperture, but the relative order is kept for closed fractures. It can be concluded that the tool parameters from the FMI are suitable for fracture aperture computation from the TBEI image.

A Geological Characterization Case Study from Oklahoma

This case study is from the STACK Play of the Anadarko Basin, Oklahoma, USA. The horizontal target zone is within the Mississippian age Lower Meramec Formation. The Meramec is generally considered to have been deposited as prograding lowstand clinoforms of predominantly detrital siliciclastics, with shales and minor detrital carbonates, from a carbonate-siliciclastic rimmed shelf.

The bedding boundaries, cross beddings and faults are picked with the true dip-based picking method. The TST index is computed from bedding boundaries. Correlation analysis from the GR displayed as TST reference is challenging. The relatively high GR is taken as a local geological marker, and GR shape is the secondary reference. Layer thicknesses change relatively quickly, either because of the depositional environment variation or because of incorrect dip picking. Based on the above principles, the formation correlation is achieved and shown in Figure 6: the top geological marker is defined at the bottom of the GR interval, and another marker is defined at the top of the lower GR interval; the thickness between these two markers varies along the logged interval.

The fault throws (Table 1) are estimated by assuming the TST of the same formation is relatively consistent in the near-wellbore area. Four relatively major faults are classified based on image features, and the estimated fault throws are small and even less than 1.5 ft vertically in one of the faults. The fault order is assigned based on estimated vertical throw.

After the formation correlation and fault throw estimation are completed, the structure is reconstructed from bedding boundaries and faults with the improved structural modeling method mentioned previously (Figure 7). In general, the structure in this study area is a relatively flat

monocline from northwest to southeast and north to south in some intervals. The structural dip is less than 5° in most intervals and only varies around relatively major faults at the bottom of the hole, where the dip is more than 10°.

Based on image fracture features, there are three different fracture patterns in three different electrical facies (Figure 8). The three electrical facies are siltstone, massive shale (middle section of Figure 8b and top interval of Figure 8d) and nodular shale (Figure 8e).

The first fracture pattern is developed in the siltstone, shown in Figure 8a, with a continuous feature cross-cutting the entire borehole section. The second fracture pattern is that fracture intensity is more pronounced in the siltstone beds, but only a few fractures are continuous through both the siltstone and massive shale beds, as shown in Figure 8b, Figure 8c, and Figure 8d. The third pattern is that few continuous fractures are developed in nodular shale, with short trace-length, lithology bound fractures within the highly resistive nodules.

The fracture segments are extracted automatically from the borehole image with a state-of-the-art method. The fracture aperture is computed on the TBEI image by adopting the same tool parameters with the FMI tool; the fracture density and apparent porosity are then calculated accordingly (Figure 9). From the computed fracture parameters, we see that the conductive fractures are more developed in the siltstone or shale interval with relatively lower clay volume shale. In addition to conductive fractures, there are a few resistivity fractures developed in the massive shale interval. The fracture pattern is consistent with interpreted facies changes along the well trajectory.

Based on the selected continuous conductive fractures (representing open fractures), the strike of fractures is almost west-east oriented and consistent with the present maximum horizontal stress indicated by drilling induced fractures (Figure 10). However, the strike of the resistive fractures (representing closed fractures) is rotated by approximately 45° from the present maximum horizontal stress. Based on the regional geological setting, much of the faulting, including a significant strike-slip overprint across the Anadarko Basin, and associated fracturing occurred during the Pennsylvanian. It is believed that the Pennsylvanian tectonics formed much of the fracturing, and then fractures were charged with hydrocarbons. Because most faults are strike-slip faults, it is not easy to identify them based on a two-dimensional borehole image and more faults are represented as normal or reverse faults as showing in Table 1. The relationship between present maximum horizontal stress and fracture azimuth is a good indicator for open vs. closed fracture classification by integrating borehole image features.

From the two-dimensional cross section (Figure 11), the relationship between fracture development and faults is not obvious. Most fractures are developed in intervals of low clay content, especially below horizon 2. The fracture aperture in the formation layer between horizon 2 and 3 varies significantly throughout the logged interval. The fracture aperture at the top interval is much larger than that bottom one.

Based on the above structural analysis and fracture evaluation, five intervals were classified for hydraulic fracture design, as shown in Figure 9. Seventeen stage zones were designed in later hydraulic fracturing by the integrating well trajectory. The Instantaneous Shut-in Pressure (ISIP) has close relationship with lithology and natural fracture development (Figure 9). The zone with the most natural fractures has the lowest ISIP. A layer with the same lithology, such as the interval between horizons 2 and 3 (Figure 11) has a similar ISIP. The ISIP of the interval with high clay content is slight lower than that of the formation with low clay content; this could be caused by greater development of lamination in the high clay content formation, and the closed fractures that are easily reopened by hydraulic fracturing. We do not have a good understanding of

the high ISIP that occurs at the top of the interval, although the lithology is similar to the interval at the top of borehole. The well had very good production of up to 1375 BOE/D on average in the first month after hydraulic fracturing.

Conclusions

The new through-the-bit logging electrical image tool generates a high-quality image after advanced processing that includes a new time-based speed correction algorithm. Advanced interpretation tools have been developed for this TBEI borehole image, including dip picking based on true dip and correlation analysis in a TST display. A new structural modeling method is introduced to handle multiple faults with continuous formation layers. Fracture aperture computation from this new borehole image is validated by comparison with the image from the FMI imaging tool.

This image interpretation workflow was applied to a horizontal well in an unconventional reservoir. The workflow demonstrates how advanced structural analysis, driven by an innovative new image-based dip picking methodology, can provide a more accurate representation of the wellbore position within the structural section along the length of the horizontal. By following this method, natural fractures and facies variations along the lateral can be more confidently tied to structure and ultimately, aid in optimization of the completion design on a well-by-well basis.

References Cited

Bammi, S., P. Wells, M. Fredette, J. Toniolo, A. Mallick, H. Nguyen, E. Haddad, R. Laronga, and J. Kherroubi, 2016, A New Slim Full Bore Electrical Micro-Imaging Tool Conveyed through the Drill String and Bit for Geological and Reservoir Characterization of Unconventional Reservoirs: Presented at Unconventional Resources Technology Conference, San Antonio, Texas, USA, 1-3 August, doi: 10.15530/urtec-2016-2430509

Doll, H.G, 1951, The Laterolog: A New Resistivity Logging Method with Electrodes using an Automatic Focusing System: Petroleum Transactions, AIME, v. 192, p. 305-316.

Etchecopar, A. and J.L. Bonnetain, 1992, Cross Sections from Dipmeter Data: AAPG Bulletin, v. 76/5, p. 621-637, doi: 10.1306/bdff888a-1718-11d7-8645000102c1865d.

Ma, L., Y. Li, G. Wei, S. Yang, T. Yamada, A. He, I. Le Nir, and F. Wu, 2018, A Novel Approach for Structural Delineation with Multiple Faults from High Resolution Borehole Image Dips: Presented at Gastech 2018 Conference & Exhibition, Barcelona, SPAIN, November 17-20.

Yamada, T., I. Le Nir, E. Moscardi, and A. Etchecopar, 2016, A New Parallel Fold Construction Method from Borehole Dip for Structural Delineation: AAPG Annual Conference & Exhibition, Calgary, Alberta, Canada, June 19-22. Website accessed December 17, 2018. http://www.searchanddiscovery.com/abstracts/html/2016/90259ace/abstracts/2366659.html

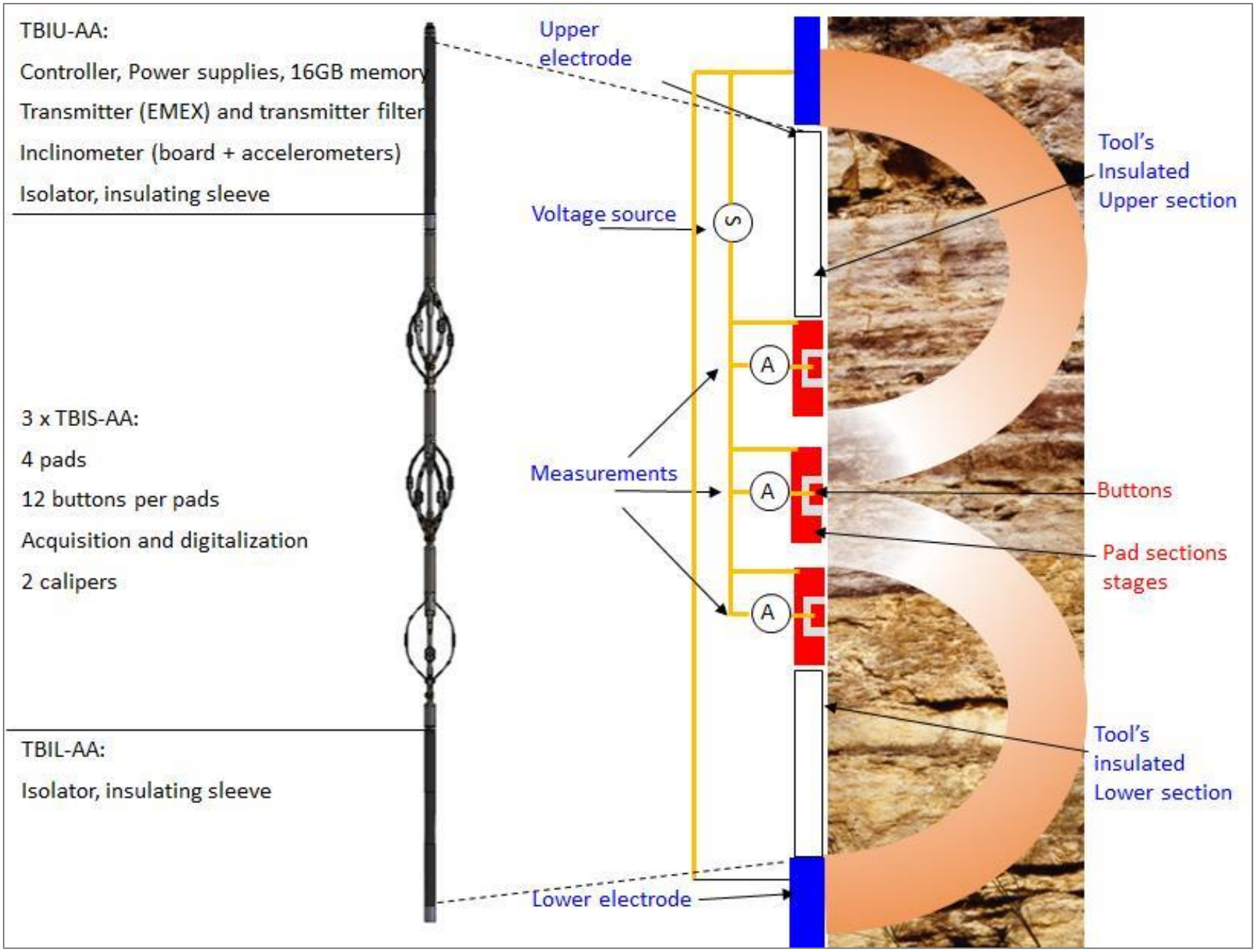

Figure 1. TBEI image tool design and measurement principle.

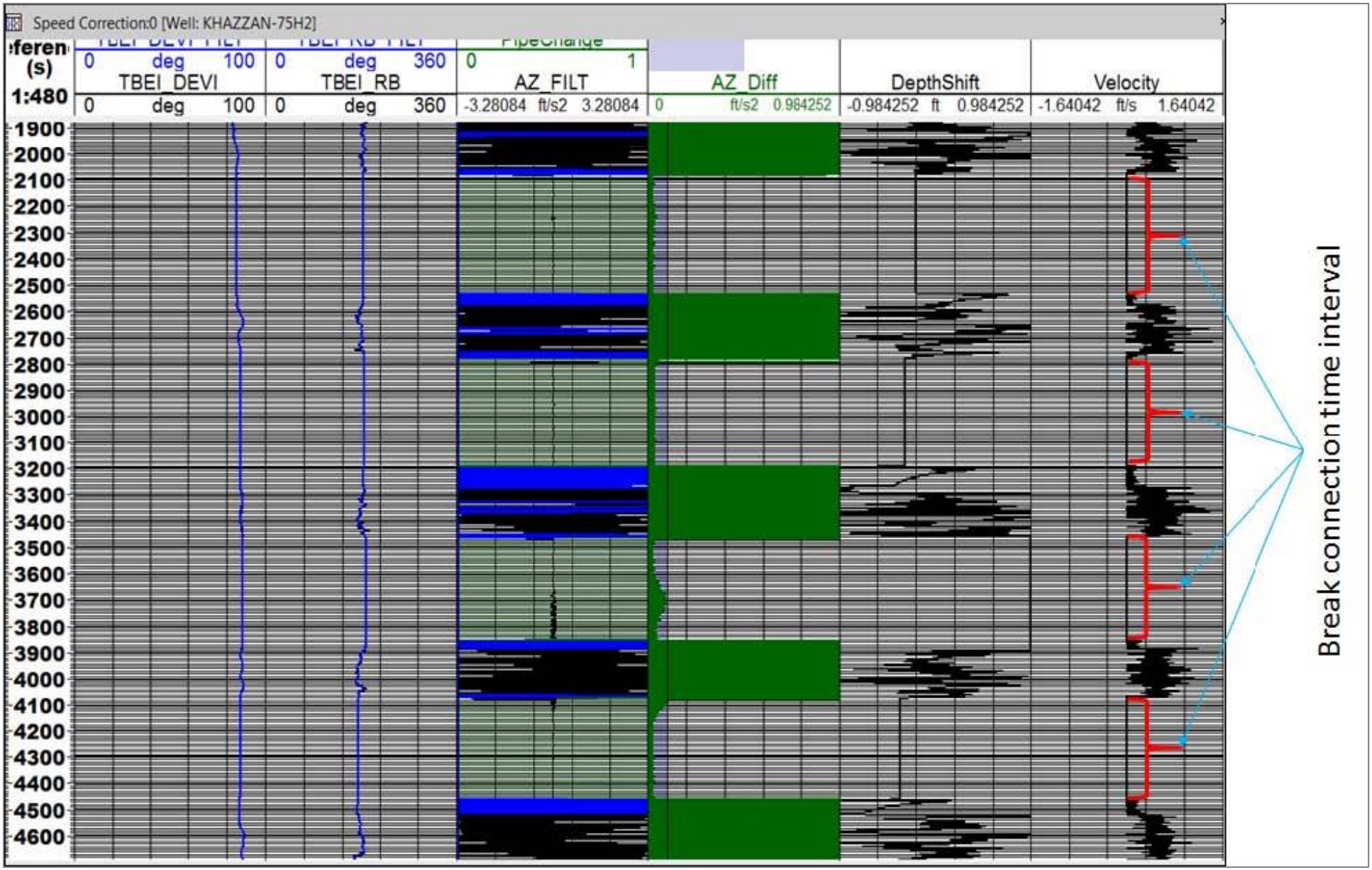

Figure 2. Specially designed speed correction solution for through-the-bit logging. Track 1, time reference; track 2, filtered acceleration (Az) and stick- slip time intervals in blue; track 3, closed Az difference; track 4, shift depth; track 5, velocity.

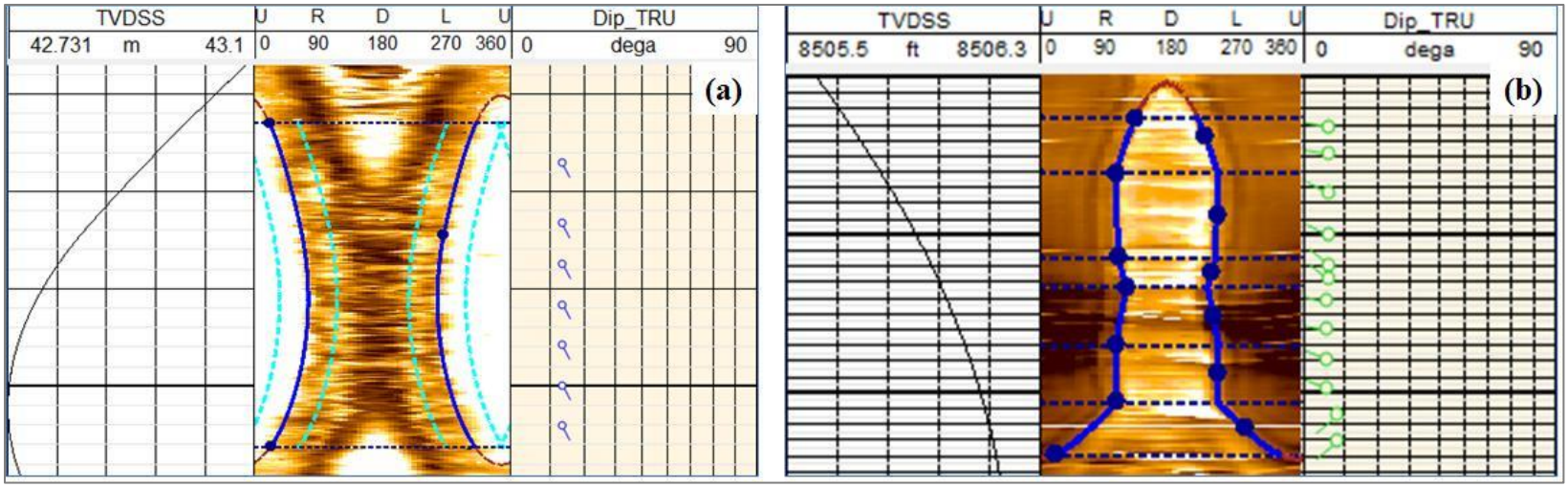

Figure 3. Dip picking based on true dip. (a) the true dip plane is defined with the first three points for a bull's eye feature. (b) Dip picking continues by following the true dip plane for a reverse bull's eye feature.

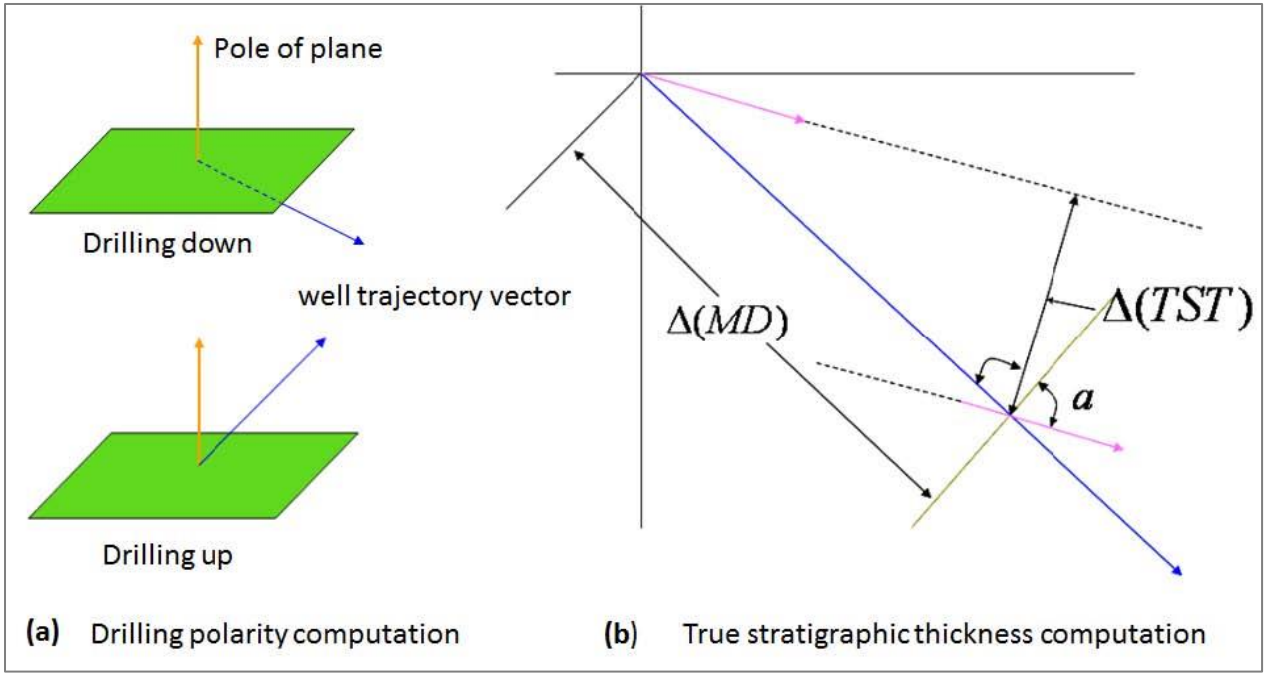

Figure 4. True drilling polarity and true stratigraphic thickness computation.

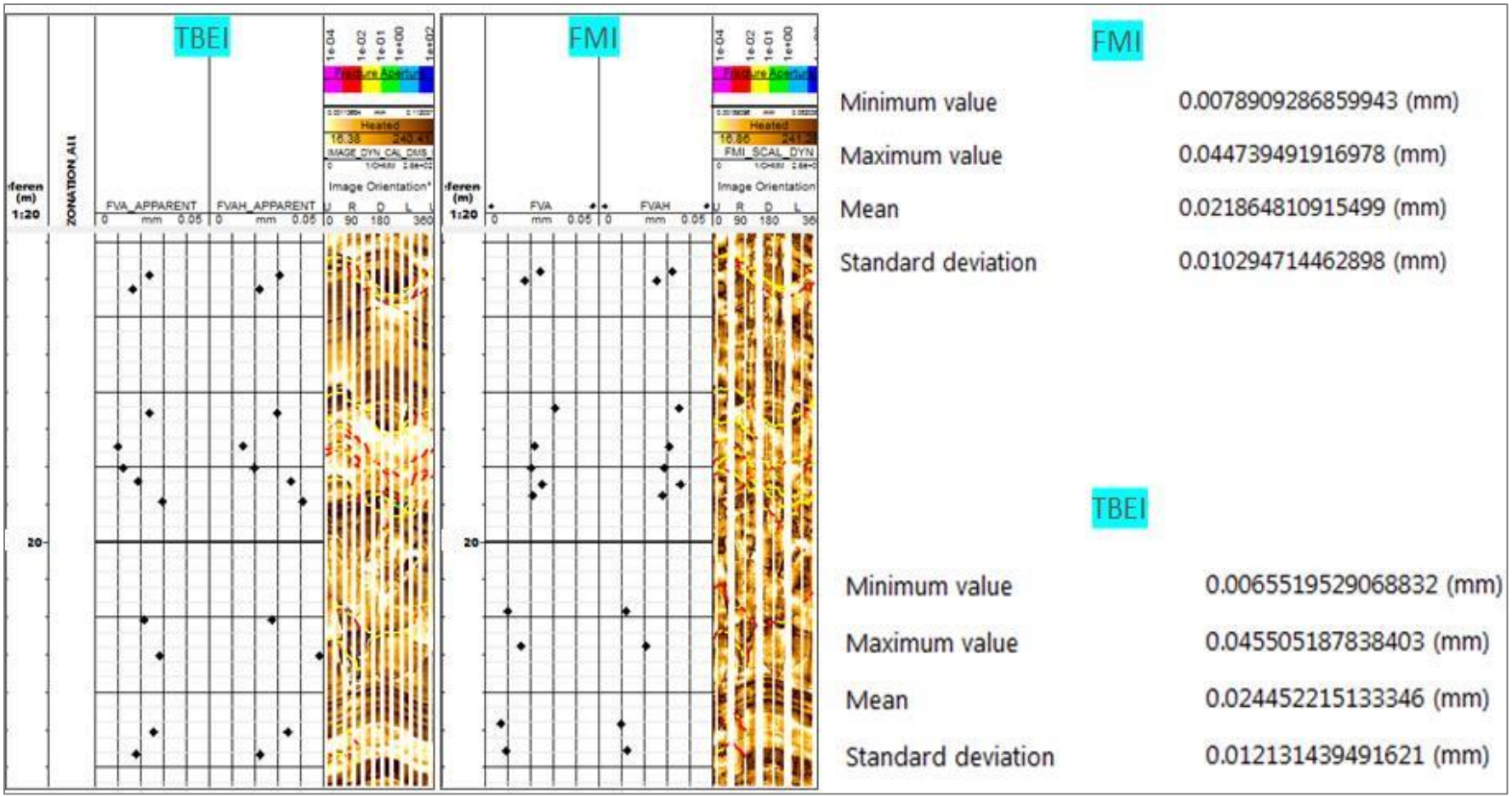

Figure 5. Fracture aperture comparison between the FMI imager and TBEI tool. Track 1, depth reference; track 2, fracture aperture from the TBEI image; track 3, hydraulic fracture aperture from the TBEI image; track 4, TBEI image; track 5, fracture aperture from the FMI image; track 6, hydraulic fracture aperture from the FMI image; track 7, the FMI image.

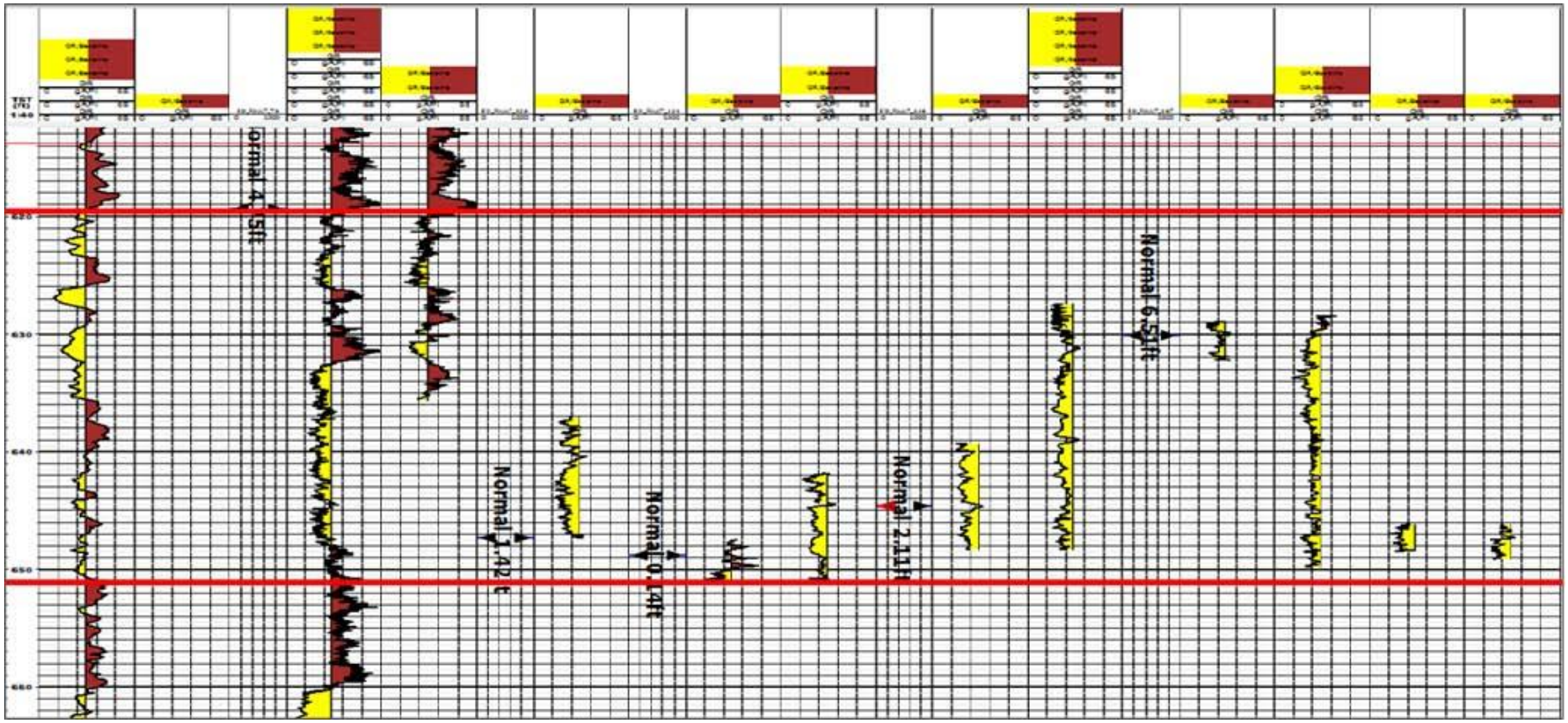

Figure 6. Correction analysis based on gamma ray curve in TST reference display.

Depth	Dip Azimuth	Dip Angle	Fault Plane Throw	Fault TST Throw	Fault Vertical Throw	Order
ft	degree	degree	ft	ft	ft	
XX469.66	100.2809	85.36956	5.537616	4.745618	6.950784	1
XX632.86	239.1072	78.40054	2.429233	1.415122	1.430324	4
XX849.77	342.9896	50.4113	6.46119	2.109604	2.207112	3
XX188.42	192.1525	59.68198	8.296527	6.51282	6.529875	2

Table 1. Fault throw estimation from correlation analysis.

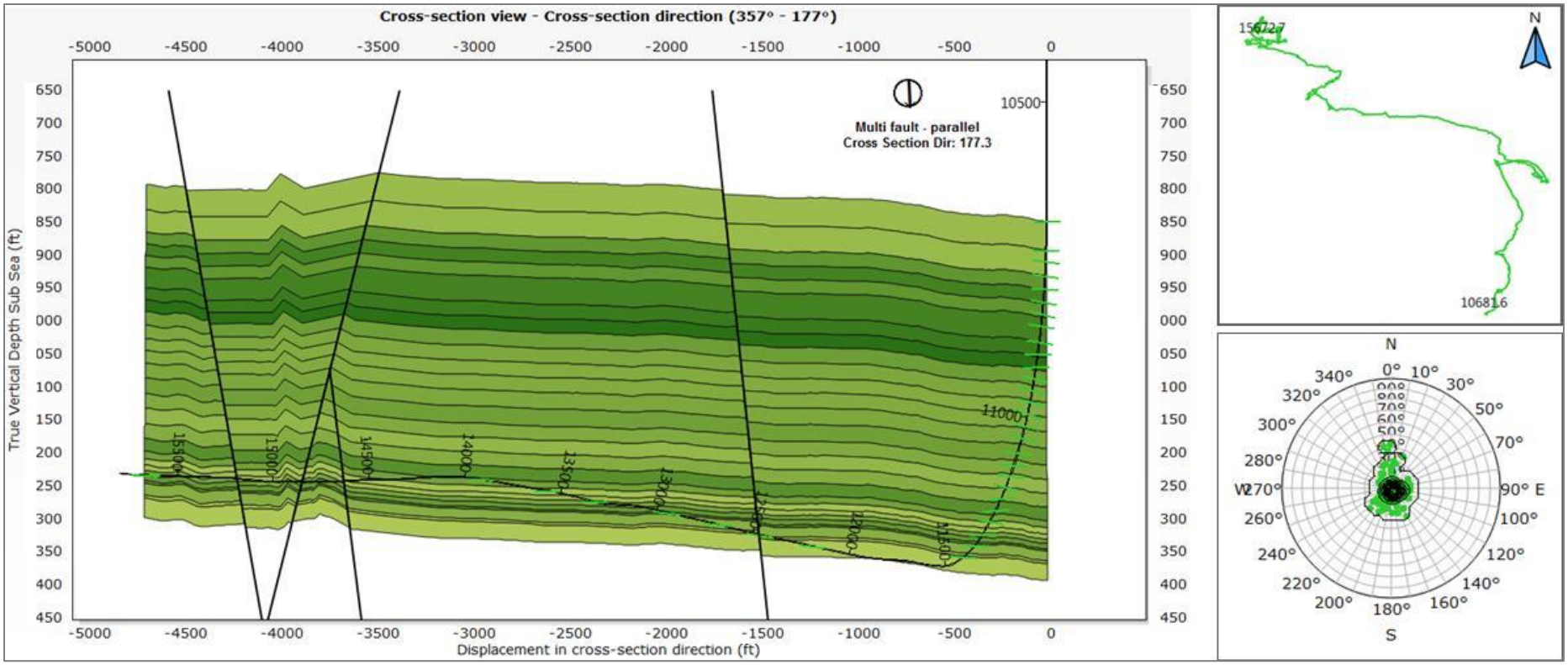

Figure 7. Structural delineation based on bedding boundary and fault dips. Left, two-dimensional reconstructed structure; top right, azimuth vector plot of bedding boundary; bottom right, bedding boundary displayed in a stereonet.

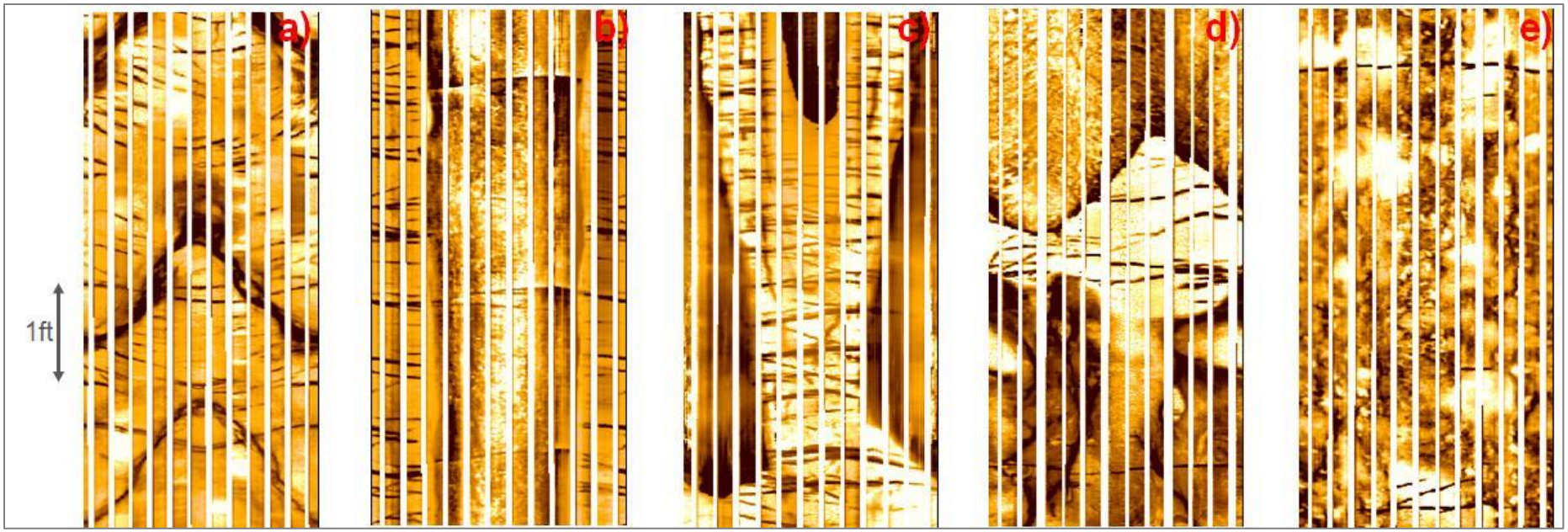

Figure 8. Different fracture patterns in the borehole image: (a) continuous fractures in siltstone; (b) lithology-bounded fracture segments with a few continuous fractures; (c) lithology-bounded continuous fractures in siltstone; (d) continuous fractures in siltstone and shale; (e) continuous fractures in shale and nodules, and fracture segments in resistive nodules. Note all images are oriented as top of hole; brighter colors represent relatively more resistive material, darker colors represent relatively more conductive material. Fractures appear conductive as they are likely open and filled with conductive water-based mud.

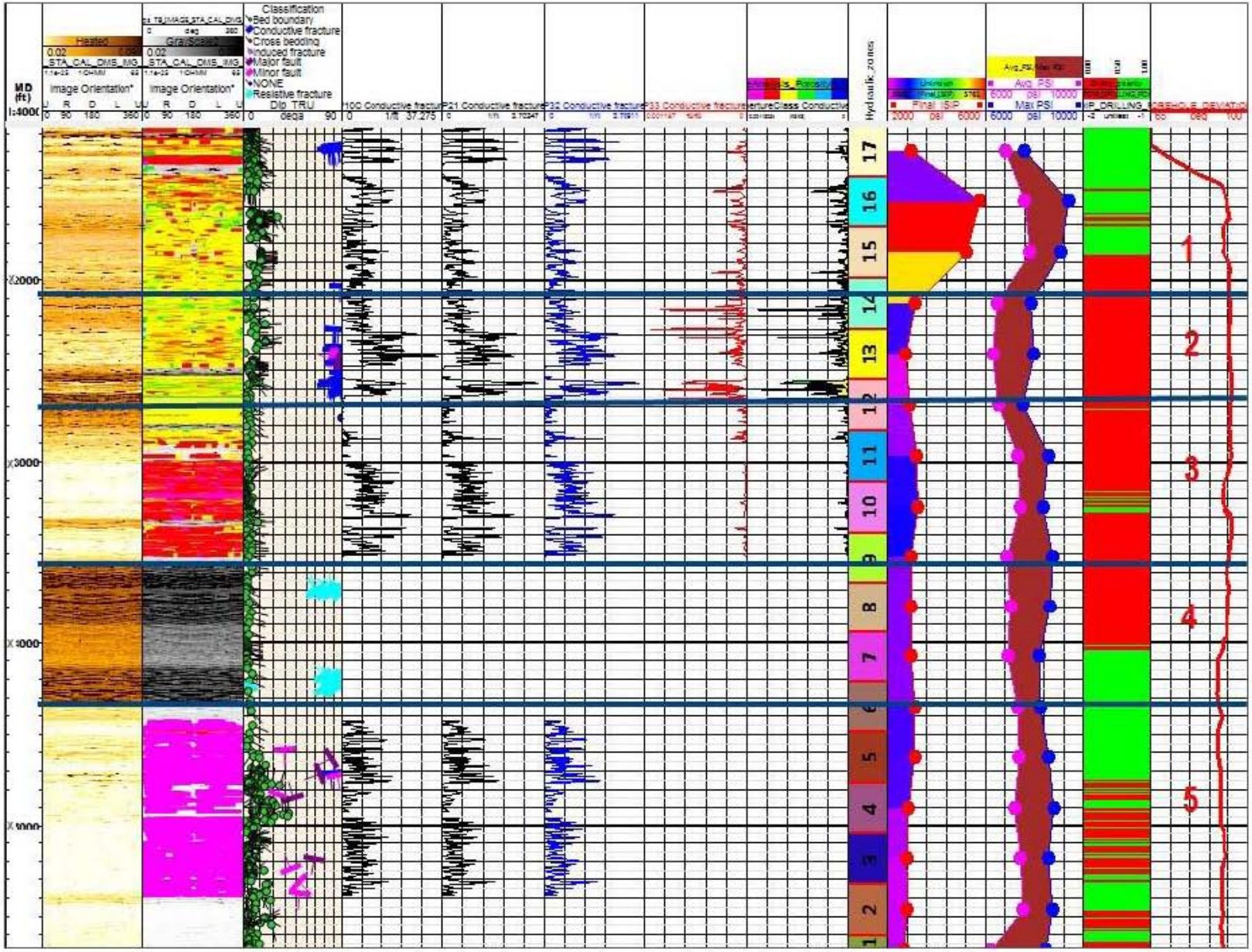

Figure 9. Fracture evaluation from borehole image. Track 1, depth reference; track 2, static borehole image; track 3, colored fracture based on aperture and gray scale borehole image; track 4, picked/classified dips; track 5, well trajectory corrected fracture density; track 6, areal fracture intensity; track 7, volumetric fracture intensity; track 8, fracture porosity; track 9, fracture aperture; track 10, hydraulic stage zones; track 11, instantaneous shut-in pressure (ISIP); track 12, average and maximum pumping pressure; track 13, drilling polarity; track 14, borehole deviation.

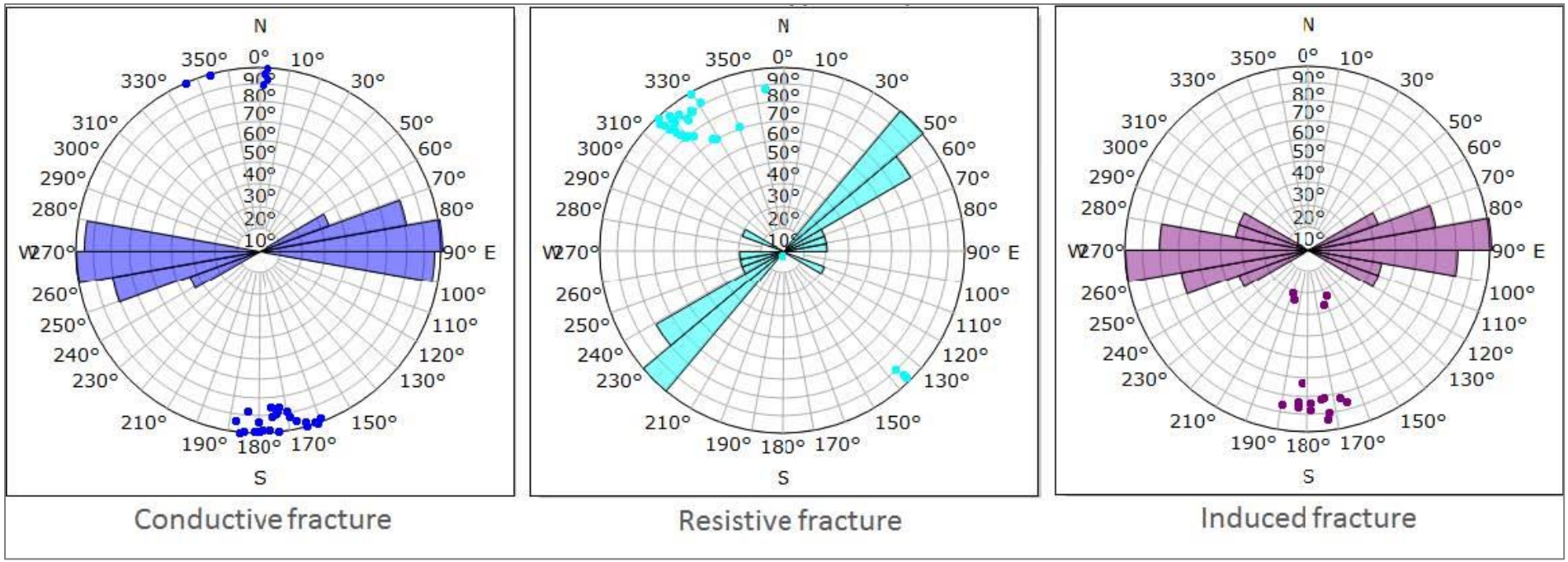

Figure 10. Fracture strike statistics. (left) The strike of selected continuous conductive fractures; (middle) The strike of continuous resistive fractures; (right) Strike of drilling induced fractures.

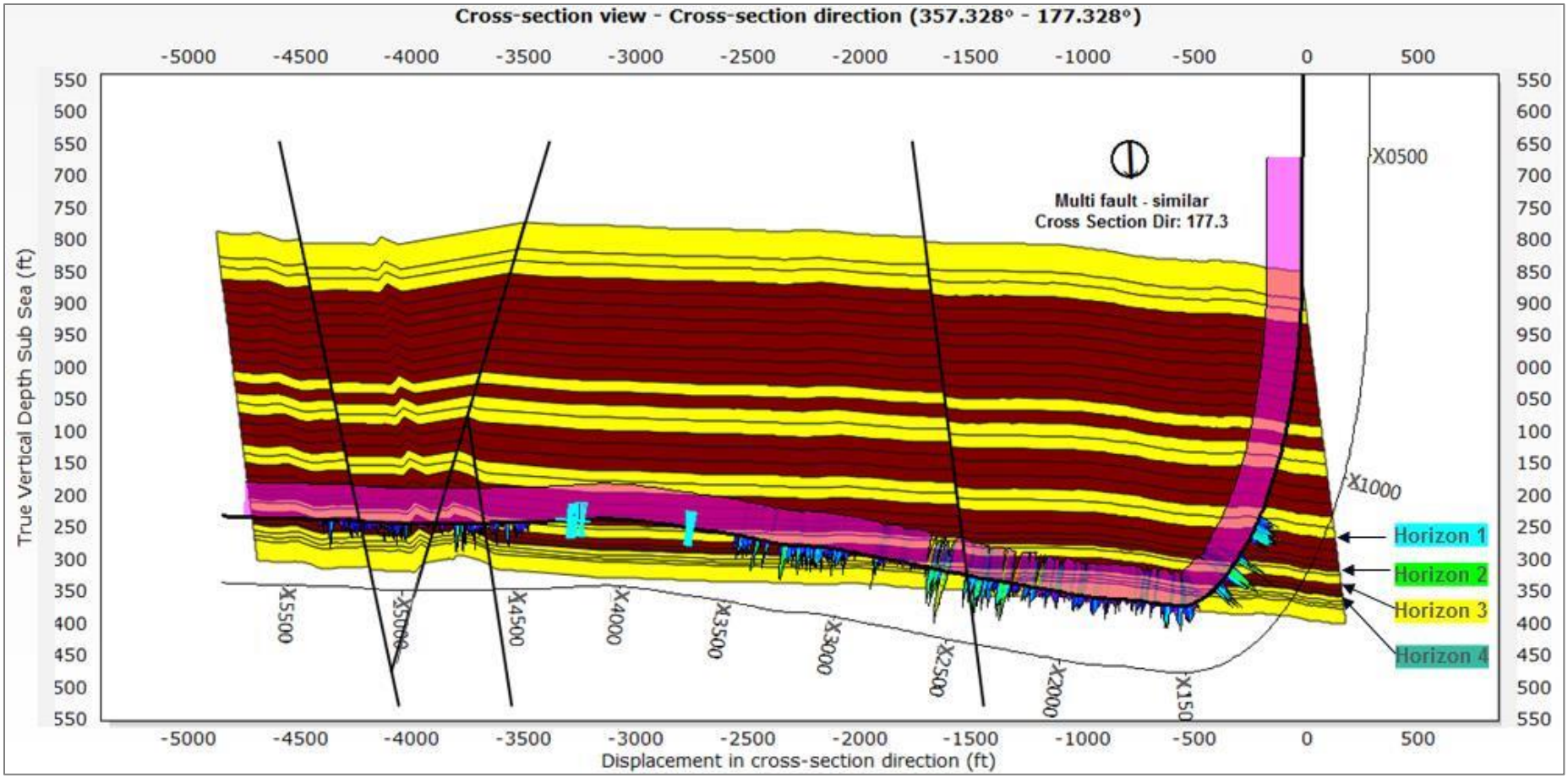

Figure 11. Structural cross section with fracture evaluation parameter logs. The log with pink background is fracture aperture and the other one is volumetric fracture intensity.